Food Chemistry: X 20 (2023) 100994

Contents lists available at ScienceDirect

Food Chemistry: X

journal homepage: www.sciencedirect.com/journal/food-chemistry-x

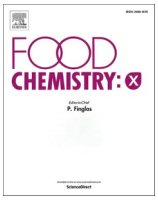

Transmembrane behaviors and quantitative structure–activity relationship of dietary flavonoids in the presence of intestinal digestive products from different carbohydrate sources based on *in vitro* and *in silico* analysis

Xiaojing Liu [a,b], Shuang Ma [a], Yuanyue Zhang [a], Yishan Fu [a,c,*], Shengbao Cai [a,*]

[a] Faculty of Food Science and Engineering, Kunming University of Science and Technology, Kunming, Yunnan Province 650500, People's Republic of China
[b] School of Food Science and Technology, Jiangnan University, Wuxi, Jiangsu Province 214122, People's Republic of China
[c] Science Center for Future Foods, Jiangnan University, Wuxi, Jiangsu Province 214122, People's Republic of China

ARTICLE INFO

Keywords:
Bioavailability
Dietary flavonoids
Wheat flour
Rice flour
In vitro simulated digestion
3D-QSAR

ABSTRACT

Bioavailability plays a key role for flavonoids to exert their bioactivities. This study investigated the transmembrane transport behavior and structure–activity of dietary flavonoids. Results showed that the apparent permeability coefficients of some flavonoids could be significantly increased when digestion products from rice flour (RD) or wheat flour (WD) are present ($p < 0.05$), especially in the WD, potentially due to higher reducing sugar ($p < 0.05$). 3D-QSAR revealed that the hydrogen bond acceptor groups at positions 5 and 6 of ring A, small-volume groups at position 3′, hydrophobic groups at position 4′, and large-volume groups at position 5′ of ring B increased the transmembrane transport of flavonoids in the WD. A hydrogen bond donor group at position 4′ of ring B enhanced the transmembrane transport of flavonoid compounds in the RD. These findings contribute to our comprehensive understanding of flavonoid absorption within the context of intestinal carbohydrate digestion.

1. Introduction

Plant polyphenols are a prominent category of secondary metabolites, encompassing various subgroups, such as flavonoids, phenolic acids and lignans. Notably, flavonoids are one of the most abundant and noteworthy subclasses (Pandey & Rizvi, 2009). Epidemiological studies have demonstrated that the consumption of a plant-based diet rich in flavonoids can exert a significant contribution to the alleviation and prevention of certain diseases, particularly those with chronic metabolic syndromes (Arfaoui, 2021; Garzón, Narváez-Cuenca, Vincken, & Gruppen, 2017; Zhang et al., 2018). However, current researches highlight the fact that many dietary flavonoids show a low bioavailability with a poor absorption (Marín, Miguélez, Villar, & Lombó, 2015; Truzzi, Tibaldi, Zhang, Dinelli, & D′Amen, 2021). Although the growing body of research emphasizes the crucial involvement of the colon in the transformation of polyphenols, it is imperative to acknowledge that these processes of absorption and conversion inherently remain limited in their scope and efficacy (Espín, González-Sarrías, & Tomás-Barberán, 2017). Since high bioavailability is a prerequisite for the fulfillment of physiological functions of substances, concerns have emerged concerning how dietary flavonoids manifest their biological activities while exhibiting such low bioavailability. This apparent contradiction has posed a challenge for researchers and remains a domain necessitating further elucidation.

Upon careful review of prior research, it becomes evident that many investigations have primarily focused on evaluating the bioaccessibility of flavonoids in an isolation system, often neglecting the simultaneous presence of other dietary components (Arfaoui, 2021). However, our diet is a comprehensive system encompass a confluence of flavonoids intermingled with vital macronutrients such as carbohydrates, lipids,

Abbreviations: CoMFA, Comparative molecular field analysis; CoMSIA, Comparative molecular similarity index analysis; DNS, 3, 5-dinitrosalicylic acid; SGF, simulated gastric fluid; SIF, simulated intestinal fluid; SSF, simulated salivary fluid; MTT, methyl thiazolyl tetrazolium; ONC, optimal number of principal components; P_{app}, apparent permeability coefficient; PLS, partial least square; RD, rice flour; UHPLC-QQQ-MS/MS, ultrahigh-performance liquid chromatography triple quadrupole tandem mass spectrometry; WD, wheat flour; 3D-QSAR, 3D-quantitative structure–activity relationship.

* Corresponding authors at: Faculty of Food Science and Engineering, Kunming University of Science and Technology, Kunming, Yunnan Province 650500, People's Republic of China (Y. Fu, and S. Cai).

E-mail addresses: fuyishankm@163.com (Y. Fu), caikmust2013@kmust.edu.cn (S. Cai).

https://doi.org/10.1016/j.fochx.2023.100994
Received 20 July 2023; Received in revised form 19 October 2023; Accepted 8 November 2023
Available online 11 November 2023

and proteins, each of which potentially wielding a profound impact on the bioaccessibility of flavonoids to certain levels (Pineda-Vadillo et al., 2016). For example, previous studies have suggested that the presence of carbohydrates can enhance the bioavailability of specific flavonoids (Jakobek, 2015; Schramm et al., 2003). Serra et al. (Serra, Macià, Romero, Valls, Bladé, Arola & Motilva, 2013) demonstrated that carbohydrate-rich foods amplified the uptake of proanthocyanidin monomers. Also, another study revealed that glucose could facilitate the absorption of anthocyanins found in red grape juice (Bitsch, Netzel, Frank, Strass, & Bitsch, 2004). Nevertheless, these investigations predominantly focused on the influence of specific carbohydrates on the bioavailability of individual or a limited number of flavonoids, failing to provide a comprehensive exploration of diverse carbohydrates' impact on the transmembrane transport behaviors of flavonoids characterized by distinct chemical structures. Furthermore, it remains unclear whether a structure–activity relationship exists between the effects of carbohydrates on the transmembrane transport of flavonoids, and if so, the governing principles of this relationship remain undetermined. These unresolved complexities pose a barrier to the advancement and practical implementation of dietary flavonoids to achieve optimal human health benefits.

Rice and wheat are typical sources of carbohydrates in the human diet. Consequently, the primary objective of this investigation was to use the Caco-2 single-cell model in conjunction with Ultrahigh-performance liquid chromatography triple quadrupole tandem mass spectrometry (UHPLC-QQQ-MS/MS) to detect the transmembrane characteristics of numerous common dietary flavonoids when subjected to the influence of intestinal digestion products originating from different carbohydrates sources (rice flour and wheat flour). Following that, 3D-Quantitative structure–activity relationship (3D-QSAR) modeling was employed to further elucidate the structure–activity relationship between various carbohydrate digestion products and the transmembrane behaviors exhibited by dietary flavonoids. The results of this investigation are expected to provide valuable insights into the bioavailability of dietary flavonoids, which may potentially advance their application in food and health product sectors. Additionally, it is anticipated that these discoveries may provide recommendations and perspectives for individuals regarding their dietary patterns.

2. Materials and methods

2.1. Materials and reagents

The standard materials (purity ≥ 98.0 %) of 22 dietary flavonoids were purchased from Chengdu Manster Biological Company, and the structure of the flavonoids used is shown in Table 1. Rice flour and

Table 1
The structures of 22 tested dietary flavonoids.

NO	Compounds	Main structure	R3	R5	R6	R7	R8	R2′	R3′	R4′	R5′
1	Baicalein	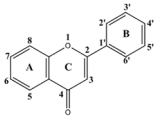	H	OH	OH	OH	H	H	H	H	H
2	Apigenin		H	OH	H	OH	H	H	H	OH	H
3*	Apigenin-7-*O*-glucoside		H	OH	H	Oglu	H	H	H	OH	H
4	Galangin		OH	OH	H	OH	H	H	H	H	H
5*	Quercetin		OH	OH	H	OH	H	H	OH	OH	H
6	Kaempferol-7-*O*-*β*-glucoside		OH	OH	H	Oglu	H	H	H	OH	H
7	Myricetin		OH	OH	H	OH	H	H	OH	OH	OH
8*	Myricitrin		Orha	OH	H	OH	H	H	OH	OH	OH
9	Isorhamnetin		OH	OH	H	OH	H	H	OMe	OH	H
10*	Isorhamnetin-3-*O*-rutinoside		ORG	OH	H	OH	H	H	OMe	OH	H
11	Vitexin		H	OH	H	OH	Glu	H	H	OH	H
12	Quercitrin		Orha	OH	H	OH	H	H	OH	OH	H
13	Naringenin	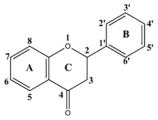	H	OH	H	OH	H	H	H	OH	H
14	Naringin		H	OH	H	Orha	H	H	H	OH	H
15	Dihydromyricetin		OH	OH	H	OH	H	H	OH	OH	H
16	Hesperetin		H	OH	H	OH	H	H	OH	OMe	H
17	Taxifolin		OH	OH	H	OH	H	H	OH	OH	H
18	Genistein	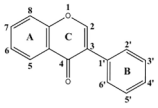	–	OH	H	OH	H	H	H	OH	H
19	Formononetin		–	H	H	OH	H	H	H	OMe	H
20*	(+)-Catechin	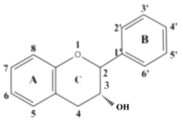	OH	OH	H	OH	H	H	H	OH	OH
21	(-)-Epicatechin	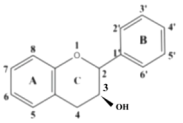	OH	OH	H	OH	H	H	H	OH	OH
22*	Cyanidin-3-*O*-glucoside	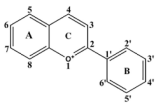	Oglu	OH	H	OH	H	H	OH	OH	H

*a randomly selected test set.

wheat flour were purchased from Ma Peizhong Agricultural Products Processing and Management Company (Henan, China), and the Caco-2 cell line was obtained from the Cell Bank of the Chinese Academy of Sciences (Kunming, China). DMEM medium, phosphate buffer solution (PBS), and Hank's balanced salt solution (HBSS) were purchased from Thermo Fisher Scientific (Gibco) (New York, USA); 12-well Transwell cell culture plates, 96-well cell culture plates, cell culture dishes, and fetal bovine serum (FBS) were purchased from Corning Inc. (New York, USA). Penicillin-streptomycin antibiotic mixture (double antibody), pancreatin solution, methylthiazolyl tetrazolium (MTT), and cell grade dimethyl sulfoxide (DMSO) were purchased from Solarbio (Beijing, China). Porcine pepsin, porcine pancreatin, sodium cholate salt and α-amylase were purchased from Merck Life Sciences (Sigma) (Shanghai, China). Laboratory water was ultrapure, and other chemicals and solvents were of analytical grade.

2.2. *In vitro simulated intestinal digestion*

In this study, an *in vitro* digestion method was used to generate digestion products from rice flour (RD) and wheat flour (WD), adapted with slight modifications from previous studies (Huang, Ma, Zhang, Cai, & Pang, 2017; Pineda-Vadillo et al., 2017). Prior to simulating digestion, simulated salivary fluid (SSF), simulated gastric fluid (SGF), and simulated intestinal fluid (SIF) were prepared according to established protocols. The composition of each simulated digestive fluid for each stage of digestion is given in Table S1. The stepwise process for *in vitro* simulated digestion is as follows:

(1) Oral digestion step: A mixture of SSF (17.5 mL), calcium chloride (0.3 M, 125 μL), α-amylase solution (1500 U/mL, 2.5 mL) and ultrapure water (4.9 mL) was combined with either 25.0 g of rice or wheat flour. The mixture was stirred in darkness at 37 °C for 2 min, yielding in simulated oral digestion samples with a concentration of 1.0 g/mL.
(2) Gastric digestion stage: the sample from the oral phase was mixed with gastric fluid (SGF) in a volume of 37.5 mL, and supplemented with 0.3 M calcium chloride (25 μL). The pH was carefully adjusted to 3.0 using 1 M hydrochloric acid, and pepsin (10.0 mL, 20,000 U/mL) was subsequently added. The system was gently stirred at a temperature of 37 °C, shielded from light, for a duration of 2 h, with a rotation speed of 100 revolutions per minute.
(3) Intestinal digestion stage: SIF (55.0 mL), 0.3 M calcium chloride (200 μL) and bile salt (resulting in a final concentration of 10.0 mM) were added to the gastric digestion sample. The pH was meticulously adjusted to 7.0 using a 1 M sodium hydroxide solution. Porcine pancreatin solution (25.0 mL, 800 U/mL) was then added and the mixture was carefully homogenized. The volume was then adjusted to 200 mL with water and the system was stirred in a light-shielded environment at a temperature of 37 °C for 2 h with a rotation speed of 100 rpm.
(4) At the end of intestinal digestion, a portion of the solution was carefully transferred to a tube containing 2.0 mL of ethanol for subsequent analysis of reducing sugars (kept at 4 °C until analysis). The remaining part of the solution was terminated by adjusting the pH to 3.0 with 1.0 M hydrochloric acid. After centrifugation, the supernatant was carefully collected, concentrated by rotary evaporation, freeze-dried, and carefully stored at −20 °C for subsequent use.

2.3. *Determination of reducing sugar*

The DNS method (3, 5-dinitrosalicylic acid method) as described in a previous study (Goh, Gao, Ananingsih, Ranawana, Henry, & Zhou, 2015) was employed for the determination of reducing sugars. In brief, the digestion solution underwent centrifugation at 2200 g and room temperature for 10 min. Following that, the supernatant (50 μL) was transferred to a centrifuge tube. An equivalent volume of water was used for the blank group and a 10.0 mg/mL glucose standard solution was used for the standard group. Subsequently, 0.25 mL of acetate buffer containing 1 % starch glucosidase was added to each tube. The mixture was incubated at room temperature for 30 min to facilitate the depolymerization of starch into monosaccharides. After depolymerisation, 0.75 mL of the DNS mixture, prepared by combining 0.5 mg/mL glucose, 4.0 M sodium hydroxide solution and DNS reagent in a 1:1:5 ratio, was added to the reaction mixture and the solution was then heated at 95 °C for 15 min. After cooling, the solution was diluted with 4.0 mL of water. The absorbance of the diluted solution was measured at 530 nm. The concentration of total reducing sugars was calculated as milligrams of reducing sugars per gram of food, in accordance with Equation (1).

Reducing sugar content (mg/g) = (Sample - Blank) / (Standard - Blank) × Total volume of digestion × Standard solution concentration × Dilution volume × 1/The sample weight (1).

2.4. *Construction of a Caco-2 cell transport model*

The determination of the safe concentrations of plant flavonoids, RD, and WD was conducted using the MTT method (Villalva, Jaime, Aguado, Nieto, Reglero, & Santoyo, 2018). The establishment of the Caco-2 cell model was based on a previous protocol (Luo, Fan, Zhao, Li, Wu, & Gao, 2018). Caco-2 cells were seeded at a density of 500 μL (1×10^5 cells/mL) per well in a chamber of a 12-well transwell plate, and 1 mL of medium was added to the receiving chamber. The cell cultures were maintained and incubated for 21 days, with medium changes every other day during the first week and daily changes for the subsequent two weeks. Upon the formation of a cell monolayer and when the transepithelial electrical resistance (TEER) exceeded 350 Ω, the medium was removed, and the cells were washed with HBSS buffer and equilibrated for 30 min. Subsequently, a mixture of 400 μg/mL digestion products (RD and WD) together with the optimal concentration of dietary flavonoids was added to the chamber and transported for 6 h. The control group consisted of dietary flavonoids only (no substrate group). TEER values were measured before and after the experiment to verify the integrity of the Caco-2 cell monolayer. After transport, the cell culture medium and cell layer on both sides were collected in a centrifuge tube and stored at −30 ℃ for future use.

2.5. *UHPLC–QQQ–MS/MS analysis*

The LCMS-8040 instrument, consisted of a UHPLC separation system coupled with a tandem mass spectrometry detection system, was employed for the analysis. The mass spectrometry conditions adopted in this investigation were based on a previous study with slight modifications (Ma, Cai, Jia, Sun, Yi & Du, 2020). The extracted samples after transmembrane transport were mixed in a 1:1 ratio with methanol (80 %), followed by centrifugation (10,000 g, 10 min), and the supernatant was filtered for MS detection. The mobile phases utilized in the study included formic acid water (0.1 % formic acid) as mobile phase A and acetonitrile as mobile phase B. The elution gradient utilized was as follows: 0–1 min: 5 % B; 1–5 min: 5–45 % B; 5–7 min: 45–70 % B; 7–8 min: 70–90 % B; 8–9 min: 90–5 % B; 9–10 min: 5 % B. A volume of 3 μL was injected, and the flow rate was set at 0.2 mL/min. The electrospray ion source was employed, and mass spectrometry was performed in multi-reaction monitoring (MRM) mode.

2.6. *The calculation of P_{app}*

The quantification of flavonoids was performed, and the apparent permeability coefficient (P_{app}) of the Caco-2 monolayer model was calculated. The formula for P_{app} calculation, depicted in Equation (2), is as follows:

$$P_{app}\ (cm/s) = (V/AC_0) \times (dc/dt)\ (2)$$

Where V represents the medium solution volume (L) on the receiving side, A denotes the surface area of the membrane, C_0 indicates the initial concentration of dietary flavonoids in the chamber (μmol/L), and dc/dt signifies the rate of concentration change over time in the solution in the receiving chamber (μmol/s).

2.7. 3D-QSAR study

2.7.1. Data collection

The apparent permeability coefficient (Papp) of the dietary flavonoids from the apical side (AP) of the transwell chamber to the basolateral side (BL) of the receiving chamber was transformed into $P^{PappAtoB}$ (-log ($P_{appAtoB}$)), which served as the dependent variable in the 3D-QSAR model. The 3D structures of the 22 dietary flavonoids were obtained from the National Center for Biotechnology Information (NCBI) (https://www.ncbi.nlm.nih.gov). Subsequently, the SYBYL-X2.1.1 software was utilized for energy optimization, with the lowest energy conformation serving as the dependent variable for the model. Descriptors were employed as independent variables. To construct the 3D-QSAR model, all structures were minimized using standard Tripos molecular mechanics and Gasteiger-Huckel charges, which are crucial for model development. The dataset included both a training set and a test set. For this experiment, 16 compounds were randomly selected as the training set, while 6 compounds were allocated to the test set (Gonzales, Van, Zotti, Kobayashi, Grootaert, Raes, & Smagghe, 2015a; Jia, Ma, Cheng, Zhang, & Cai, 2019).

2.7.2. Superposition of molecules

All molecules were superimposed using two benzene rings as a common skeleton. After several overlapping tests, quercitrin was chosen as the template molecule for conducting molecular alignment of the flavonoid compounds. The Align Database method was employed for this purpose.

2.7.3. Comparative molecular field analysis (CoMFA) and comparative molecular similarity index analysis (CoMSIA)

Both CoMFA and CoMSIA were employed as independent variables in the 3D-QSAR analysis with the primary objective of understanding the relationship between flavonoid structure and transmembrane transport (Gonzales et al., 2015a; Gao, Fu, Yi, Gao, Jia, & Cai, 2020). CoMFA includes two molecular fields, namely electrostatic field and steric field, while CoMSIA consists of five molecular fields: electrostatic field, steric field, hydrophobic field, hydrogen bond acceptor field, and hydrogen bond donor field. To build a more robust and accurate 3D-QSAR model, both methodologies were used for the validation purposes in this experiment.

2.7.4. Partial least square (PLS) analysis

The PLS method was employed to construct a statistically significant 3D-QSAR model, as described in previous studies (Jia et al., 2019; Li et al., 2016). Variables extracted from two descriptors from CoMFA and five descriptors from CoMSIA were used for the PLS analysis. Cross-validation was conducted using the "Leave one out" (LOO) method. The optimal number of principal components (ONC), cross-validation correlation coefficient (q^2), standard error of the estimate (SEE), fisher test value (F), and non-cross-validation coefficient (R^2) were determined through the leave-one-out method. Finally, a three-dimensional isopotential map was employed to visualize the relationship between $P^{PappAtoB}$ of flavonoids and each field.

2.8. Statistical analysis

All experiments were repeated at least twice, and the results are presented as mean ± standard deviation (S.D.). One-way ANOVA analysis was employed when the results followed a normal distribution. After confirming the homogeneity of variance using Levene's statistic, Tukey's test was conducted to evaluate significant differences ($p < 0.05$). The Origin 8.5 software (OriginLab, Northampton, MA, USA) was utilized for these statistical analyses.

3. Results and discussion

3.1. Reducing sugar determination of in vitro simulated digestion products

Our *in vivo* studies have provided compelling evidence supporting the influence of the interaction between dietary flavonoids and carbohydrates on the bioavailability of flavonoids (Neilson, Sapper, Janle, Rudolph, Matusheski, & Ferruzzi, 2010; Schramm et al., 2003). This observed effect is hypothesized to be associated with the entry or exit of glucose, the end product of carbohydrate digestion, traversing the cells of the small intestine. The presence of glucose can increase the permeability of the cell membrane, potentially facilitating the transmembrane transport of dietary flavonoids, consequently increasing their bioavailability (Hajiaghaalipour, Manizheh, & Aditya, 2015; Goh, Gao, Ananingsih, Ranawana Henry, & Zhou, 2015). In fact, the digestion rate of carbohydrates exhibits variations on their respective origins, subsequently exerting diverse influences on the transmembrane transportation of flavonoids. Within this study, an appraisal was conducted to quantify the levels of reducing sugars detected in the digestion products of rice flour and wheat flour. The results are visually depicted in Fig. S1. Notably, the reducing sugar content of RD (229.55 ± 26.56 mg/g) demonstrated a significantly discernible disparity in comparison to the WD (374.38 ± 19.59 mg/g) ($p < 0.05$). This dissimilarity may potentially be attributed to the distinctive starch compositions inherent to rice flour and wheat flour, respectively. Specifically, wheat flour encompasses a higher proportion of straight-chain starch, constituting approximately 25 %, while rice flour contains a comparatively lower percentage, approximately 18 %. Straight-chain starch, characterized by its α-1,4-glucosidic bonds, adopts a structure rendering it more susceptible to hydrolysis by α-amylase and/or α-glucosidase during oral and intestinal digestion. Consequently, this hydrolysis yields a greater production of glucose (Miao, Xu, Jia, Zhang, Niu, & Zhao, 2021). The distinct post-digestion sugar profiles of these two carbohydrates suggest that they may exhibit varying effects on flavonoid transport across cellular membranes.

3.2. Transport of dietary flavonoids under the carbohydrate intestinal digestion product system

The presence of carbohydrate constituents within food can potentially exert an influence on the transmembrane transport of dietary flavonoids following their gastrointestinal digestion. Therefore, when considering the transmembrane transport of dietary flavonoids, it becomes imperative to holistically consider the interplay between carbohydrates, particularly their intestinal digestion products, and dietary flavonoids. The widely employed Caco-2 monolayer model, derived from human colon adenocarcinoma origins, sharing a multitude of morphological attributes such as microvilli, as well as functional characteristics similar to mature enterocytes, serves as a valuable tool estimate the intestinal permeability of diverse dietary nutrients (Fang, Liang, Liu, Qaiser, & Xu, 2018). The transmembrane transit of dietary flavonoids across the Caco-2 cell membrane compartment, from the apical to the basolateral direction (A to B), is conventionally described by the apparent permeability coefficient, termed $P_{appAtoB}$. In this study, a non-toxic concentration of 40 μM was used for all dietary flavonoids, and the non-toxic concentration of RD and WD was 400 μg/mL.

As delineated in Table 2, the results show significant variability in the apparent permeability coefficients of various dietary flavonoids. Ddihydroflavonoids, including taxifolin, dihydromyricetin, and naringenin, as well as flavanols like, epicatechin and catechin, and

Table 2
Apparent permeability coefficient ($P_{appAtoB}$) of dietary flavonoids in Caco-2 monolayer.

NO	Compounds	No substrate $P_{appAtoB} \times 10^{-6}$ cm/s	RD $P_{appAtoB} \times 10^{-6}$ cm/s	Increase in $P_{appAtoB}$	WD $P_{appAtoB} \times 10^{-6}$ cm/s	Increase in $P_{appAtoB}$
1	Baicalein	2.89 ± 0.03^{b}	2.28 ± 0.01^{a}	−0.21	3.79 ± 0.10^{c}	0.31
2	Apigenin	1.64 ± 0.02^{a}	3.13 ± 0.01^{b}	0.90	4.18 ± 0.06^{c}	1.54
3	Apigenin-7-*O*-glucoside	5.75 ± 0.05^{a}	6.37 ± 0.02^{a}	0.11	11.24 ± 0.64^{b}	0.95
4	Galangin	6.86 ± 0.02^{a}	8.76 ± 0.01^{b}	0.28	12.01 ± 0.49^{c}	0.75
5	Quercetin	9.22 ± 0.08^{b}	6.54 ± 0.03^{a}	−0.29	10.83 ± 0.25^{c}	0.18
6	Kaempferol-7-*O*-*β*-glucoside	0.64 ± 0.05^{a}	1.26 ± 0.02^{b}	0.96	3.67 ± 0.15^{c}	4.71
7	Myricetin	5.55 ± 0.02^{a}	9.07 ± 0.01^{b}	0.63	17.79 ± 0.03^{c}	2.21
8	Myricitrin	6.25 ± 0.09^{b}	5.55 ± 0.07^{a}	−0.11	10.82 ± 0.31^{c}	0.73
9	Isorhamnetin	9.32 ± 0.09^{b}	6.64 ± 0.03^{a}	−0.29	11.42 ± 0.91^{c}	0.23
10	Isorhamnetin-3-*O*-rutinoside	7.78 ± 0.05^{b}	5.40 ± 0.09^{a}	−0.31	11.68 ± 0.07^{c}	0.50
11	Vitexin	28.53 ± 0.05^{c}	25.87 ± 0.04^{b}	−0.09	15.54 ± 0.46^{a}	−0.46
12	Quercitrin	5.60 ± 0.08^{b}	1.47 ± 0.05^{a}	−0.73	9.61 ± 0.28^{c}	0.72
13	Naringenin	12.64 ± 0.05^{b}	5.43 ± 0.06^{a}	−0.57	11.15 ± 1.54^{b}	−0.12
14	Naringin	1.35 ± 0.08^{a}	1.80 ± 0.01^{b}	0.34	2.38 ± 0.09^{c}	0.77
15	Dihydromyricetin	17.30 ± 0.07^{c}	16.38 ± 0.03^{b}	−0.05	14.82 ± 0.15^{a}	−0.14
16	Hesperetin	7.28 ± 0.09^{b}	1.98 ± 0.02^{a}	−0.73	12.18 ± 0.53^{c}	0.67
17	Taxifolin	24.84 ± 0.08^{c}	15.66 ± 0.09^{a}	−0.37	17.71 ± 0.43^{b}	−0.29
18	Genistein	11.93 ± 0.10^{a}	14.45 ± 0.09^{b}	0.21	22.89 ± 0.09^{c}	0.92
19	Formononetin	23.76 ± 0.09^{c}	12.01 ± 0.01^{a}	−0.49	22.68 ± 0.95^{b}	−0.05
20	(+)-Catechin	11.22 ± 0.06^{a}	18.75 ± 0.09^{b}	0.67	10.77 ± 0.07^{a}	−0.04
21	(-)-Epicatechin	23.04 ± 0.09^{a}	37.30 ± 0.04^{c}	0.62	27.24 ± 0.45^{b}	0.18
22	Cyanidin-3-*O*-glucoside	7.96 ± 0.08^{a}	7.85 ± 0.07^{a}	−0.01	7.97 ± 0.06^{a}	0.00

$P_{appAtoB}$ values were expressed as mean ± SD (n = 3). Different letters on the same line (a, b, c) indicated significant differences ($p < 0.05$). RD:Rice flour digested products, WD: Wheat flour digested products.

isoflavones, such as formononetin, displayed notably higher apparent permeability coefficients. In contrast, the transmembrane conveyance of flavonols, exemplified by kaempferol-7-*O*-*β*-glucoside, as well as flavones like baicalein and apigenin, was observed to be comparatively poor. The lower $P_{appAtoB}$ of flavonols, such as kaempferol-7-*O*-*β*-glucoside, may be attributed to the presence of a glycosidic bond, the hydroxyl group at position 3, as well as the number and positioning of hydrogen bond donors and acceptors in these compounds (Hollman & Arts, 2000; Çelik & Koşar, 2012; Gonzales et al., 2015a). Additionally, it is noteworthy that vitexin showcased the highest apparent permeability coefficient, potentially due to its distinctive glycosidic bond position (R8), necessitating further investigation for conclusive insights.

In the system of carbohydrate intestinal digestion products, the transmembrane transport behaviors of dietary flavonoids may be influenced by the type of carbohydrate and the inherent transport capabilities of the flavonoids themselves. Table 2 illustrates the varying effects exerted by RD and WD on the transmembrane transport of flavonoids. In the RD group, flavonoids possessing inherent good permeability, such as isoflavones and dihydroflavones, showed no an augmentation but rather demonstrated a declining trend. Conversely, for the majority of dietary flavonoids with an average passage rate, their apparent permeability coefficient experienced a discernible increase ($p < 0.05$). For instance, myricetin showed a remarkable 0.63-fold increase in its apparent permeability coefficient compared to the substrate-free group. Notably, the apparent permeability coefficients of the less permeable flavonoids, namely apigenin, naringin, and kaempferol-7-*O*-*β*-glucoside, exhibited significant enhancements of 0.90-fold, 0.34-fold, and 0.96-fold, respectively, compared to the substrate-free group. The WD group manifested a comparable trend to the RD group, with an even more pronounced increase in the apparent permeability coefficient compared to the substrate-free group. In addition to flavonoids known for their inherently high permeability, such as vitexin, naringenin, dihydromyricetin, taxifolin, formononetin and catechin, other flavonoids exhibited varying degrees of improvement. Specifically, kaempferol-7-*O*-*β*-glucoside exhibited a remarkable 4.71-fold increase in its apparent permeability coefficient within the WD system, compared to the substrate-free group. Some compounds experienced a decrease in the apparent permeability coefficient within the RD group but showed an increase in the WD group, as observed for baicalein and myricitrin. In conclusion, the presence of rice or wheat flour tends to enhance the transmembrane transport of most flavonoids in the system. This enhancement may be mediated by the carbohydrate-specific effects on the gastrointestinal motility, secretion, or the activity of a carbohydrate-flavonol transporter (Zhang, Yu, Sun, Liu, Jiang, Guo, & Ren, 2014). Furthermore, the magnitude of this influence on the transmembrane translocation of dietary flavonoids is closely related to the structural properties of the flavonoids themselves (Wang, Wu, Yang, Yang, & Wang, 2011). Therefore, to gain further insights into the relationship between transmembrane behavior and structural properties of dietary flavonoids, an investigation using the 3D-QSAR model was conducted under different conditions of carbohydrate digestion products.

3.3. Results and analysis of CoMFA and CoMSIA

In this study, a comprehensive analysis encompassed a total of 22 dietary flavonoids employing the 3D-QSAR approach, under varying conditions representing different carbohydrate digestion product substrates including no substrate group, RD group, and WD group. Two different methods, CoMFA and CoMSIA, were used to construct the models. The flavonoids were separated into a training set comprising 16 flavonoids and a test set comprising 6 flavonoids. Molecular superposition was facilitated using quercitrin as the template molecule (shown in Fig. 1 (a)), and the CoMFA and CoMSIA models were generated using compounds from the training set. Table 3 showcases both the predicted apparent permeability coefficient values ($P^{PappAtoB}$) and the corresponding true values for all 22 flavonoids. Concurrently, Fig. 1 (b) exhibits a scatter plot, was facilitated illustrating a robust linear correlation between the predicted and true values. This indicates the strong predictive capability of the CoMFA and CoMSIA models.

The statistical parameters of the CoMFA model are outlined in Table S2. The q^2 values, serving as indicators of the model's predictive aptitude, were determined to be 0.505, 0.548, and 0.505 for the no substrate group, RD group, and WD group, respectively. All these values surpass the threshold of 0.5, signifying the robust predictive capabilities and overall reliability of the model. The ONC was determined to be 3, 6, and 6 for the no substrate group, RD group, and WD group, respectively and the corresponding R^2 values obtained with the ONC approach were 0.982, 0.994, and 0.997 respectively. Additionally, the SEE values were determined to be 0.075, 0.047, and 0.022, respectively. The F-test values obtained for the models were 224.294, 242.946, and 545.141, all

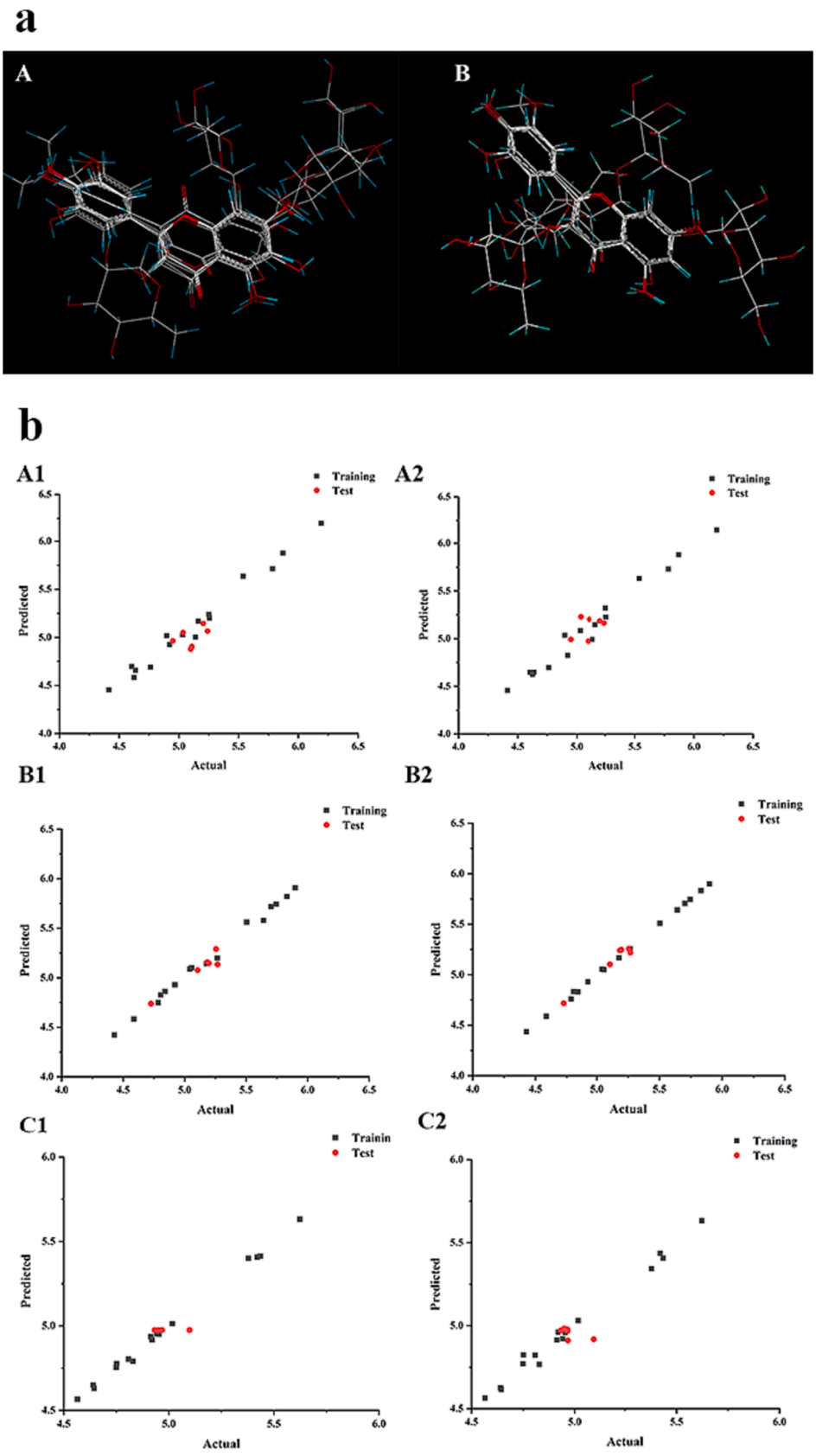

Fig. 1. (a) Molecular superposition diagram of CoMFA (A) and CoMSIA (B). Quercitrin was used as a template molecule. (b) Scatter plots of predicted and true $P^{PappAtoB}$ values generated by CoMFA (1) and CoMSIA (2) models. The letters A, B, and C represent no substrate group, RD group, and WD group, respectively. RD: Rice flour digested products, WD: Wheat flour digested products.

Table 3
Actual and predicted $P^{PappAtoB}$ values of dietary flavonoids generated from 3D-QSAR models.

NO	Compounds	No substrate $P^{PappAtoB}$	Pred 1	Residual	Pred 2	Residual	RD $P^{PappAtoB}$	Pred 1	Residual	Pred 2	Residual	WD $P^{PappAtoB}$	Pred 1	Residual	Pred 2	Residual
1	Baicalein	5.5386 ± 0.0045	5.6349	−0.0963	5.6307	−0.0921	5.6416 ± 0.0021	5.5780	0.0636	5.6410	0.0006	5.4210 ± 0.0115	5.4073	0.0137	5.4359	−0.0149
2	Apigenin	5.7840 ± 0.0053	5.7130	0.0710	5.7301	0.0539	5.5045 ± 0.0017	5.5620	−0.0575	5.5090	−0.0045	5.3788 ± 0.0062	5.4000	−0.0212	5.3435	0.0353
3*	Apigenin-7-*O*-glucoside	5.2402 ± 0.0035	5.0650	0.1752	5.1650	0.0752	5.1962 ± 0.0012	5.1460	0.0502	5.2460	−0.0498	4.9494 ± 0.0248	4.9750	−0.0256	4.9830	−0.0336
4	Galangin	5.1635 ± 0.0015	5.1678	−0.0043	5.1466	0.0169	5.0577 ± 0.0006	5.1010	−0.0433	5.0500	0.0077	4.9203 ± 0.0177	4.9177	0.0026	4.9607	−0.0404
5*	Quercetin	5.0353 ± 0.0036	5.0500	−0.0147	5.2300	−0.1947	5.1846 ± 0.0018	5.1560	0.0286	5.2390	−0.0544	4.9652 ± 0.0100	4.9750	−0.0098	4.9770	−0.0118
6	Kaempferol-7-*O*-*β*-glucoside	6.1924 ± 0.0339	6.2008	−0.0084	6.1523	0.0401	5.8996 ± 0.0075	5.9080	−0.0084	5.9000	−0.0004	5.4355 ± 0.0178	5.4129	0.0226	5.4074	0.0281
7	Myricetin	5.2557 ± 0.0016	5.2016	0.0541	5.2259	0.0298	5.0423 ± 0.0005	5.0890	−0.0467	5.0540	−0.0117	4.7498 ± 0.0007	4.7537	−0.0039	4.7700	−0.0202
8*	Myricitrin	5.2041 ± 0.0065	5.1450	0.0591	5.1850	0.0191	5.2555 ± 0.0021	5.2900	−0.0345	5.2570	−0.0015	4.9657 ± 0.1302	4.9750	−0.0093	4.9680	−0.0023
9	Isorhamnetin	5.0308 ± 0.0044	5.0263	0.0045	5.0844	−0.0536	5.1776 ± 0.0056	5.1430	0.0346	5.1680	0.0096	4.9422 ± 0.0347	4.9532	−0.0110	4.9207	0.0215
10*	Isorhamnetin-3-*O*-rutinoside	5.1092 ± 0.0029	4.9040	0.2052	5.2020	−0.0928	5.2680 ± 0.0069	4.9340	0.3340	5.2180	0.0500	4.9324 ± 0.0025	4.9750	−0.0426	4.9710	−0.0386
11	Vitexin	4.4142 ± 0.0005	4.4530	−0.0388	4.4555	−0.0413	4.5872 ± 0.0007	4.5840	0.0032	4.5870	0.0002	4.8085 ± 0.0129	4.8034	0.0051	4.8225	−0.0140
12	Quercitrin	5.2517 ± 0.0064	5.2378	0.0139	5.3211	−0.0694	5.8305 ± 0.0144	5.8200	0.0105	5.8310	−0.0005	5.0172 ± 0.0127	5.0128	0.0044	5.0315	−0.0143
13	Naringenin	4.8983 ± 0.0017	5.0182	−0.1199	5.0346	−0.1363	5.2656 ± 0.0048	5.1970	0.0686	5.2550	0.0106	4.9528 ± 0.0604	4.9511	0.0017	4.9575	−0.0047
14	Naringin	5.8706 ± 0.0258	5.8794	−0.0088	5.8785	−0.0079	5.7447 ± 0.0029	5.7420	0.0027	5.7450	−0.0003	5.6234 ± 0.0164	5.6310	−0.0076	5.6322	−0.0088
15	Dihydromyricetin	4.7620 ± 0.0018	4.6910	0.0710	4.6947	0.0673	4.7857 ± 0.0008	4.7490	0.0367	4.7610	0.0247	4.8292 ± 0.0044	4.7908	0.0384	4.7675	0.0617
16	Hesperetin	5.1381 ± 0.0054	5.0043	0.1338	4.9931	0.1450	5.7033 ± 0.0053	5.7190	−0.0157	5.7060	−0.0027	4.9145 ± 0.0189	4.9361	−0.0216	4.9151	−0.0006
17	Taxifolin	4.6049 ± 0.0015	4.6968	−0.0919	4.6462	−0.0413	4.8052 ± 0.0025	4.8270	−0.0218	4.8330	−0.0278	4.7518 ± 0.0105	4.7770	−0.0252	4.8245	−0.0727
18	Genistein	4.9234 ± 0.0035	4.9262	−0.0028	4.8239	0.0995	4.8401 ± 0.0028	4.8620	−0.0219	4.8300	0.0101	4.6404 ± 0.0017	4.6501	−0.0097	4.6255	0.0149
19	Formononetin	4.6242 ± 0.0017	4.5817	0.0425	4.6250	−0.0008	4.9205 ± 0.0005	4.9290	−0.0085	4.9300	−0.0095	4.6444 ± 0.0182	4.6315	0.0129	4.6162	0.0282
20*	(+)-Catechin	4.9500 ± 0.0021	4.9630	−0.0130	4.9920	−0.0420	4.7270 ± 0.0100	4.7380	−0.0110	4.7170	0.0100	4.9676 ± 0.0030	4.9750	−0.0074	4.9110	0.0566
21	(-)-Epicatechin	4.6375 ± 0.0017	4.6571	−0.0196	4.6473	−0.0098	4.4283 ± 0.0005	4.4220	0.0063	4.4350	−0.0067	4.5648 ± 0.0071	4.5662	−0.0014	4.5641	0.0007
22*	Cyanidin-3-*O*-glucoside	5.0993 ± 0.0045	4.6790	0.4203	4.9730	0.1263	5.1052 ± 0.0038	5.0770	0.0282	5.1020	0.0032	5.0987 ± 0.0033	4.9750	0.1237	4.9180	0.1807

RD:Rice flour digested products, WD: Wheat flour digested products.
$P^{PappAtoB}$ values are expressed as mean ± SD (n = 3), Pred1. means predicted $P^{PappAtoB}$ values of CoMFA; Pred 2. means predicted $P^{PappAtoB}$ values of CoMSIA. CoMSIA, comparative similarity index analysis; CoMFA, comparative molecular field analysis.
*The randomly selected test set.

exceeding 100, indicating an exceptionally significant fit for the models. These statistical parameters convincingly indicate that the 3D-QSAR model has a strong fit and predictive ability. Notably the CoMFA model reveals varying contributions from the steric field and hydrophobic field under different substrate conditions. The steric field contributions in the CoMFA model were 44.5 %, 38.6 % and 42.1 % for the no-substrate group, RD group and WD group, respectively, and the electrostatic field contributions were 55.5 %, 61.4 % and 57.9 %, respectively.

Within the CoMSIA model, the q^2 values corresponding to different substrate conditions (no substrate group, RD group, and WD group) were determined to be 0.533, 0.530, and 0.669, respectively. All these values exceed 0.5, indicating of the robust predictive ability and reliability of the model. The ONC for each substrate condition was determined as 4, 9, and 4, respectively. The R^2 values determined by the ONC approach were 0.979, 0.999, and 0.990 for the no substrate group, RD group, and WD group, respectively. The SEE values were calculated as 0.085, 0.019, and 0.037, respectively, for the three substrate conditions. The F-test values observed were 129.895, 1052.629, and 273.444 for the no substrate group, RD group, and WD group, respectively, all surpassing the threshold of 100. Based on these statistical parameters, it can be confidently concluded that the 3D-QSAR model exhibits strong fitting ability and robust prediction capacity. Within the CoMSIA model, the contributions of the steric field, electrostatic field, hydrophobic field, and hydrogen bond donor–acceptor field exhibit variations under different substrate conditions. Specifically, the contributions of the steric field were determined to be 8.3 %, 7.2 %, and 8.0 % for the no substrate group, RD group, and WD group, respectively. Additionally, the contribution values of the electrostatic field were found to be 26.3 %, 30.4 %, and 24.2 %, while the hydrophobic field contributed 20.6 %, 16.2 %, and 18.1 %, and the hydrogen bond donor–acceptor field contributed 44.800 %, 46.200 %, and 49.600 %, respectively, within the same three groups.

3.4. 3D isopotential map analysis of CoMFA and CoMSIA models

Fig. 2 (a) and Fig. 2 (b) show the 3D isopotential maps generated by the CoMFA and CoMSIA analyses. These visual representations utilize encompassing color blocks surrounding the molecule to elucidate the influence of molecular fields on the permeability of flavonoids as they across the Caco-2 cell layer. To optimize the visual clarity of the color block diagram, a template molecule, quercitrin, was selected as a reference and shown from an equivalent viewpoint. CoMFA and CoMSIA models across different substrate conditions. Notably, a conspicuous expansion of the vibrant cluster was observed at the 7 position of the A ring, implying that the introduction of big groups at this site could enhance the activity of the respective compounds. One illustrative example is the augmented transmembrane transport ability of apigenin-7-*O*-glucoside relative to apigenin, both in the absence and presence of a carbohydrate matrix, attributed to the presence of a substantial group, namely O-glucosidic, at position 7. The presence of blue color blocks within the electrostatic field indicates that the incorporation of electron-donating groups at this particular site can enhance the activity of the compound. The red color blocks indicate the presence of electron-withdrawing groups. Notably, there is a prominent expansion of the blue color around the 3 position of the C ring in this model, indicating that the introduction of electron donor groups at this location amplifies the activity of the compound. This phenomenon can be attributed to the unique structural characteristics of flavonoids, particularly the presence of a double bond at positions 2 and 3 of the C ring, facilitating a strong conjugation effect. In addition, a significant area of red color appears at the 7 position of ring A, particularly in the WD group. This signifies that the aggregation of electron-withdrawing groups at this specific location may potentially contribute to the favorable biological activity of flavonoids.

Within the CoMFA model, compared to the no substrate group, the presence of the green group was predominantly observed at the R5′ position in both the RD and WD groups, with a notable prominence in the WD group. This elucidates the improved activity displayed by myricetin and myricitrin in the presence of a carbohydrate matrix, thereby enabling more efficient cellular penetration under the influence of the wheat flour matrix. Additionally, the CoMSIA model suggested that the appearance of the yellow group was noted at the 4′ position of the B ring and the 3 position of the C ring in the no substrate group. This indicates that a small volume group at this position contributes to the activity of the compound. Interestingly, in the RD and WD groups, yellow groups were not only identified at the 3 position of the C ring but also extended to occupy the B ring, particularly in the WD group. This finding elucidates the enhanced activity displayed by apigenin, galangin, kaempferol-7-*O*-glucoside, and naringin in the WD group. These specific compounds feature small groups at both the 3′ and 4′ positions of the C ring, as well as the 3′ and 4′ positions of the B ring. Within the hydrogen bond donor field, the presence of a hydrogen bond donor, such as a hydroxyl group, at the positions characterized by a cyan color

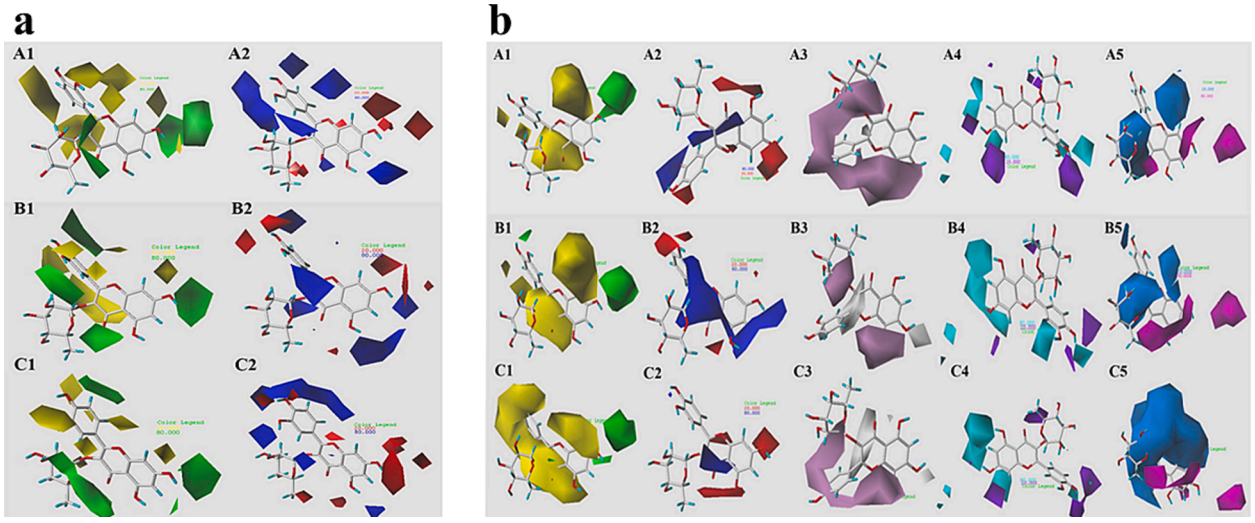

Fig. 2. 3D isopotential diagram of CoMFA model (a) and CoMSIA model (b). The letters A, B, and C represent no substrate group, RD group, and WD group, respectively. The numbers 1, 2, 3, 4, and 5 represent the steric field, electrostatic field, hydrophobic field, hydrogen bond donor field, and hydrogen bond acceptor field, respectively. RD: Rice flour digested products, WD: Wheat flour digested products.

contributes to the enhanced activity of the compound. The cyan color was observed at the 6 and 8 positions of the A ring, as well as the 3′ position of the B ring, in all three matrix groups. In addition, cyan was also noted at the 4′ position of the B ring in the RD group. In the hydrogen bond acceptor field, the introduction of the magenta group at the positions where the hydrogen bond acceptor is present increases the activity of the compound. Magenta was observed at the 4 and 7 positions of the C ring in all three matrix groups. Furthermore, in the RD and WD groups, magenta was also present at positions 5 and 6 of the A ring.

Moreover, the appearance of purple color in the hydrophobic field indicates that the presence of a hydrophobic group at a specific position augments the activity of the compound. Interestingly, in this study, a consistent purple color was observed at position 8 of the A ring across all three matrix groups and the WD group exhibited a larger volume at this position compared to the RD group. This finding provides an explanation for the lower activity observed in vitexin compared to other compounds in the presence of a carbohydrate matrix, especially within the WD group. Vitexin, derived from the substitution of the 8 position of apigenin with glucoside, encompasses multiple hydroxyl groups, contributing to the increased hydrophilicity of flavonoids. Interestingly, the presence of the purple group was also noted at the 4′ position of the B ring within the WD group, but not in the RD group. This elucidates the observed decrease in permeability of hesperetin and formononetin in the RD group, while their permeability increases in the WD matrix. This phenomenon can be attributed to the presence of a methoxyl group at the R4′ position, known for its hydrophobic properties. Previous studies have emphasized the significant improvement in the transmembrane transport ability of plant flavonoids when hydroxyl groups undergo methylation, which is consistent with our findings (Gonzales, Smagghe, Grootaert, Zotti, Raes, & Camp, 2015b). Moreover, the analysis of isopotential maps revealed notable distinctions in the positions of hydrogen bond donors and acceptors between the RD and WD groups, in comparison to the no substrate group, particularly at the 5 and 6 positions of ring A. This disparity likely represents a significant contributing factor influencing the improved transmembrane transport of plant flavonoids observed in the RD and WD scenarios. Notably, a previous study has highlighted that the number and positioning of hydrogen bond donors and acceptors play a crucial role in influencing the transmembrane transport of flavonoids in Caco-2 cell models (Gonzales et al., 2015a).

3.5. *Structure-activity relationship analysis of 3D-QSAR*

In this study, a 3D-QSAR analysis was performed to explore the mechanisms governing the transmembrane transport of dietary

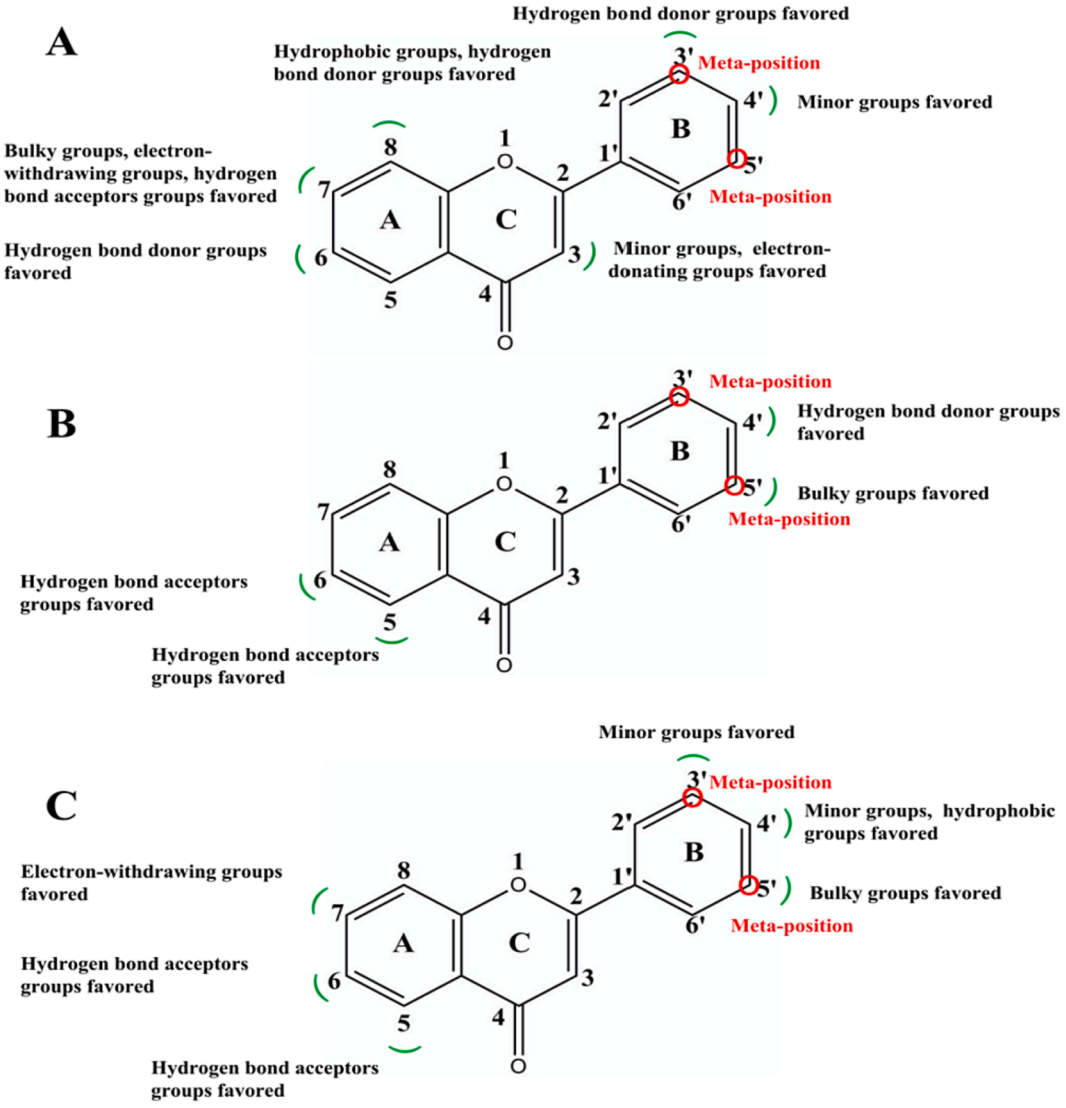

Fig. 3. 3D-QSAR quantitative structure–activity relationship analysis of dietary flavonoids under different carbohydrate systems. The letters A, B, and C represent no substrate group, RD group, and WD group, respectively. RD: Rice flour digested products, WD: Wheat flour digested products.

flavonoids in the presence of different carbohydrate digestion products. The results enabled us to establish a comprehensive structure–activity relationship, as illustrated in Fig. 3. The specific structure–activity relationship can be summarized as follows: 1) The transmembrane transport of dietary flavonoids in the no-substrate system was found to be facilitated by the presence of minor and electron-donating groups at the 3 positions of the C ring. Additionally, a hydrogen bond donor group at the 6 position of the A ring, bulky, electron-withdrawing, and hydrogen bond receptor groups at position 7 of the A ring, hydrophobic and hydrogen bond donor groups at position 8 of the A ring, and a hydrogen bond donor group at the 3′ position of the B ring were also found to contribute to the transport process. Furthermore, the presence of a minor group at the 4′ position of the B ring was observed to play a significant role. 2) The transmembrane transport of dietary flavonoids in the RD system was found to be facilitated by the presence of hydrogen bond receptor groups at the 5 and 6 positions of the A ring. Additionally, a hydrogen bond donor group at the 4′ position of the B ring and a bulky group at the 5′ position of the B ring were observed to contribute to the transport process. 3) The transmembrane transport of dietary flavonoids in the WD system was found to be facilitated by the presence of hydrogen bond receptor groups at the 5 and 6 positions of the A ring. Additionally, a minor group at the 3′ position of the B ring, minor and hydrophobic groups at the 4′ position of the B ring, and a bulky group at the 5′ position of the B ring were identified as contributing to the transport process.

4. Conclusion

In summary, this study found that the transmembrane transport of dietary flavonoids is significantly influenced by the digestion products of carbohydrates. The structural characteristics of flavonoids and the content of reducing sugars in the carbohydrate digestion products system may be the main contributory factors to this influence. It was observed that both the RD and WD systems increased transmembrane transport of most dietary flavonoids. In addition, the 3D-QSAR analysis reveals that the incorporation of hydrogen bond acceptor groups at positions 5 and 6 of ring A, small-volume groups at the 3′ position of ring B, hydrophobic groups at the 4′ position of ring B, and large-volume groups at the 5′ position of ring B significantly enhance the transmembrane transport of flavonoid compounds in the presence of WD system, as compared to the no-substrate system. By contrast, the presence of a hydrogen bond donor group at the 4′ position of ring B remarkably enhances the transmembrane transport of flavonoid compounds in the RD system The outcomes of this study contribute to a better understanding of how the structural properties of dietary flavonoids influence their transmembrane transport in the presence of different carbohydrates. Additionally, these findings also provide valuable insights for enhancing the bioaccessibility of dietary flavonoids under the context of various carbohydrate digestion products.

Chemical compounds studied in this article

Taxifolin (PubChem CID: 439533); Dihydromyricetin (PubChem CID: 161557); Naringenin (PubChem CID: 932); (-)-Epicatechin (PubChem CID: 72276); (+)-Catechin (PubChem CID: 9064); Formononetin (PubChem CID: 5280378); Kaempferol-7-*O*-*β*-glucoside (PubChem CID: 86576407); Baicalein (PubChem CID: 5281605); Apigenin (PubChem CID: 5280443)

CRediT authorship contribution statement

Xiaojing Liu: Conceptualization, Methodology, Investigation, Data curation, Writing – original draft, Writing – review & editing. **Shuang Ma:** Conceptualization, Methodology, Data curation, Writing – original draft, Writing – review & editing. **Yuanyue Zhang:** Conceptualization, Methodology, Investigation, Writing – review & editing. **Yishan Fu:** Conceptualization, Methodology, Validation, Writing – review & editing, Supervision. **Shengbao Cai:** Conceptualization, Validation, Writing – review & editing, Supervision.

Declaration of Competing Interest

The authors declare that they have no known competing financial interests or personal relationships that could have appeared to influence the work reported in this paper.

Data availability

Data will be made available on request.

Acknowledgments

The present work was financially supported by the National Natural Science Foundation of China (Grant No. 31960477), Basic Research Program of Yunnan Provincial Science and Technology Department (Grant No. 202001AT070032) and Yunnan Major Science and Technology Project (Grant Nos. 202202AG050009 and 202202AE090007). We are very grateful to Doctor Jianan Zhang at the University of North Carolina at Chapel Hill and Doctor Chengting Zhang at the University of Exeter for revising the language of this manuscript.

Appendix A. Supplementary data

Supplementary data to this article can be found online at https://doi.org/10.1016/j.fochx.2023.100994.

References

Arfaoui, L. (2021). Dietary plant polyphenols: Effects of food processing on their content and bioavailability. *Molecules, 26*(10), 2959. https://doi.org/10.3390/molecules26102959

Bitsch, R., Netzel, M., Frank, T., Strass, G., & Bitsch, I. (2004). Bioavailability and biokinetics of anthocyanins from red grape juice and red wine. *Journal of Biomedicine and Biotechnology, 2004*(5), 293. https://doi.org/10.1155/S1110724304403106

Çelik, H., & Koşar, M. (2012). Inhibitory effects of dietary flavonoids on purified hepatic NADH-cytochrome b5 reductase: Structure–activity relationships. *Chemico-biological interactions, 197*(2–3), 103–109. https://doi.org/10.1016/j.cbi.2012.04.003

Espín, J. C., González-Sarrías, A., & Tomás-Barberán, F. A. (2017). The gut microbiota: A key factor in the therapeutic effects of (poly) phenols. *Biochemical Pharmacology, 139*, 82–93. https://doi.org/10.1016/j.bcp.2017.04.033

Fang, Y., Liang, F., Liu, K., Qaiser, S., & Xu, X. (2018). Structure characteristics for intestinal uptake of flavonoids in Caco-2 cells. *Food Research International, 105* (Mar.), 353–360. https://doi.org/10.1016/j.foodres.2017.11.045

Gao, F., Fu, Y., Yi, J., Gao, A., Jia, Y., & Cai, S. (2020). Effects of different dietary flavonoids on dipeptidyl peptidase-IV activity and expression: Insights into structure–activity relationship. *Journal of Agricultural and Food Chemistry, 68*(43), 12141–12151. https://doi.org/10.1021/acs.jafc.0c04974

Garzón, G. A., Narváez-Cuenca, C. E., Vincken, J.-P., & Gruppen, H. (2017). Polyphenolic composition and antioxidant activity of açai (Euterpe oleracea Mart.) from Colombia. *Food Chemistry, 217*, 364–372. https://doi.org/10.1016/j.foodchem.2016.08.107

Goh, R., Gao, J., Ananingsih, V. K., Ranawana, V., Henry, C. J., & Zhou, W. (2015). Green tea catechins reduced the glycaemic potential of bread: An *in vitro* digestibility study. *Food Chemistry, 180*, 203–210. https://doi.org/10.1016/j.foodchem.2015.02.054

Gonzales, G. B., Van Camp, J., Zotti, M., Kobayashi, V., Grootaert, C., Raes, K., & Smagghe, G. (2015). Two-and three-dimensional quantitative structure–permeability relationship of flavonoids in Caco-2 cells using stepwise multiple linear regression (SMLR), partial least squares regression (PLSR), and pharmacophore (GALAHAD)-based comparative molecular similarity index analysis (COMSIA). *Medicinal Chemistry Research, 24*, 1696–1706. https://doi.org/10.1007/s00044-014-1241-4

Gonzales, G. B., Smagghe, G., Grootaert, C., Zotti, M., Raes, K., & Camp, J. V. (2015). Flavonoid interactions during digestion, absorption, distribution and metabolism: A sequential structure–activity/property relationship-based approach in the study of bioavailability and bioactivity. *Drug Metabolism Reviews, 47*(2), 175–190. https://doi.org/10.3109/03602532.2014.1003649

Hajiaghaalipour, F., Manizheh, K., & Aditya, A. (2015). Modulation of glucose transporter protein by dietary flavonoids in type 2 diabetes mellitus. *International journal of biological sciences, 11*(5), 508. https://doi.org/10.7150/ijbs.11241

Hollman, P. C., & Arts, I. C. (2000). Flavonols, flavones and flavanols–nature, occurrence and dietary burden. *Journal of the Science of Food and Agriculture, 80*(7), 1081–1093.

https://doi.org/10.1002/(SICI)1097-0010(20000515)80:7<1081::AID-JSFA566>3.0.CO;2-G

Huang, S., Ma, Y., Zhang, C., Cai, S., & Pang, M. (2017). Bioaccessibility and antioxidant activity of phenolics in native and fermented *Prinsepia utilis* Royle seed during a simulated gastrointestinal digestion *in vitro*. *Journal of Functional Foods, 37*, 354–362. https://doi.org/10.1016/j.jff.2017.08.004

Jakobek, L. (2015). Interactions of polyphenols with carbohydrates, lipids and proteins. *Food Chemistry, 175*, 556–567. https://doi.org/10.1016/j.foodchem.2014.12.013

Jia, Y., Ma, Y., Cheng, G., Zhang, Y., & Cai, S. (2019). Comparative study of dietary flavonoids with different structures as α-glucosidase inhibitors and insulin sensitizers. *Journal of Agricultural and Food Chemistry, 67*(37), 10521–10533. https://doi.org/10.1021/acs.jafc.9b04943

Li, Y., Chang, Y., Deng, J., Li, W., Jian, J., Gao, J., … He, R.-R. (2016). Prediction and evaluation of the lipase inhibitory activities of tea polyphenols with 3D-QSAR models. *Scientific Reports., 6*(1), 34387. https://doi.org/10.1038/srep34387

Luo, L., Fan, M., Zhao, H., Li, M., Wu, X., & Gao, W. (2018). Pharmacokinetics and bioavailability of the isoflavones formononetin and ononin and their *in vitro* absorption in ussing chamber and Caco-2 cell models. *Journal of Agricultural and Food Chemistry, 66*(11), 2917–2924. https://doi.org/10.1021/acs.jafc.8b00035

Ma, Q., Cai, S., Jia, Y., Sun, X., Yi, J., & Du, J. (2020). Effects of hot-water extract from vine tea (Ampelopsis grossedentata) on acrylamide formation, quality and consumer acceptability of bread. *Foods, 9*(3), 373. https://doi.org/10.3390/foods9030373

Marín, L., Miguélez, E. M., Villar, C. J., & Lombó, F. (2015). Bioavailability of dietary polyphenols and gut microbiota metabolism: Antimicrobial properties. *BioMed Research International, 2015*. https://doi.org/10.1155/2015/905215

Miao, L., Xu, Y., Jia, C., Zhang, B., Niu, M., & Zhao, S. (2021). Structural changes of rice starch and activity inhibition of starch digestive enzymes by anthocyanins retarded starch digestibility. *Carbohydrate Polymers, 261*(1), Article 117841. https://doi.org/10.1016/j.carbpol.2021.117841

Neilson, A. P., Sapper, T. N., Janle, E. M., Rudolph, R., Matusheski, N. V., & Ferruzzi, M. G. (2010). Chocolate Matrix Factors Modulate the Pharmacokinetic Behavior of Cocoa Flavan-3-ol Phase II Metabolites Following Oral Consumption by Sprague-Dawley Rats. *Journal of Agricultural and Food Chemistry, 58*(11), 6685–6691. https://doi.org/10.1021/jf1005353

Pandey, K. B., & Rizvi, S. I. (2009). Plant polyphenols as dietary antioxidants in human health and disease. *Oxidative Medicine and Cellular Longevity, 2*, 270–278. https://doi.org/10.4161/oxim.2.5.9498

Pineda-Vadillo, C., Nau, F., Dubiard, C. G., Cheynier, V., Meudec, E., Sanz-Buenhombre, M., … Hingyi, H. (2016). *In vitro* digestion of dairy and egg products enriched with grape extracts: Effect of the food matrix on polyphenol bioaccessibility and antioxidant activity. *Food Research International, 88*, 284–292. https://doi.org/10.1016/j.foodres.2016.01.029

Pineda-Vadillo, C., Nau, F., Guerin-Dubiard, C., Jardin, J., Lechevalier, V., Sanz-Buenhombre, M., … Dupont, D. (2017). The food matrix affects the anthocyanin profile of fortified egg and dairy matrices during processing and *in vitro* digestion. *Food Chemistry, 214*, 486–496. https://doi.org/10.1016/j.foodchem.2016.07.049

Serra, A., Macià, A., Romero, M., Valls, J., Bladé, C., Arola, L., & Motilva, M. (2013). Bioavailability of procyanidin dimers and trimers and matrix food effects in *in vitro* and *in vivo* models - CORRIGENDUM. *British Journal of Nutrition*. https://doi.org/10.1017/S000711451200596X

Schramm, D. D., Karim, M., Schrader, H. R., Holt, R. R., Kirkpatrick, N. J., Polagruto, J. A., … Keen, C. L. (2003). Food effects on the absorption and pharmacokinetics of cocoa flavanols. *Life Sciences, 73*(7), 857–869. https://doi.org/10.1016/S0024-3205(03)00373-4

Truzzi, F., Tibaldi, C., Zhang, Y., Dinelli, G., & D′ Amen, E. (2021). An overview on dietary polyphenols and their biopharmaceutical classification system (BCS). *International Journal of Molecular Sciences, 22*(11), 5514. https://doi.org/10.3390/ijms22115514

Villalva, M., Jaime, L., Aguado, E., Nieto, J. A., Reglero, G., & Santoyo, S. (2018). Anti-inflammatory and antioxidant activities from the basolateral fraction of Caco-2 cells exposed to a rosmarinic acid enriched extract. *Journal of Agricultural and Food Chemistry, 66*(5), 1167–1174. https://doi.org/10.1021/acs.jafc.7b06008

Wang, Y., Wu, Q., Yang, X. W., Yang, X., & Wang, K. (2011). The membrane transport of flavonoids from Crossostephium chinense across the Caco-2 monolayer. *Biopharmaceutics & Drug Disposition, 32*(1), 16–24. https://doi.org/10.1002/bdd.735

Zhang, H., Yu, D., Sun, J., Liu, X., Jiang, L., Guo, H., & Ren, F. (2014). Interaction of plant phenols with food macronutrients: Characterisation and nutritional–physiological consequences. *Nutrition Research Reviews, 27*(1), 1–15. https://doi.org/10.1017/S095442241300019X

Zhang, J., Zhao, L., Cheng, Q., Ji, B., Yang, M., Sanidad, K. Z., … Zhou, F. (2018). Structurally different flavonoid subclasses attenuate high-fat and high-fructose diet induced metabolic syndrome in rats. *Journal of agricultural and food chemistry, 66*(46), 12412–12420. https://doi.org/10.1021/acs.jafc.8b03574